Journal of Nuclear Materials 378 (2008) 110–119

Contents lists available at ScienceDirect

Journal of Nuclear Materials

journal homepage: www.elsevier.com/locate/jnucmat

An elastoplastic phase-field model for the evolution of hydride precipitation in zirconium. Part I: Smooth specimen

X.H. Guo [a,b], S.Q. Shi [a,*], Q.M. Zhang [b], X.Q. Ma [c]

[a] Department of Mechanical Engineering, The Hong Kong Polytechnic University, Hung Hom, Kowloon, Hong Kong
[b] State Key Laboratory of Explosion and Safety Science, Beijing Institute of Technology, Beijing 100081, China
[c] Department of Physics, University of Science and Technology Beijing, Beijing 100083, China

ARTICLE INFO

Article history:
Received 14 January 2008
Accepted 16 May 2008

ABSTRACT

An elastoplastic phase-field model was developed to simulate the morphology evolution of hydride precipitation in zirconium bulk material without flaws (considered in this part), and with flaws (considered in Part II). In the present Part I, a theoretical framework based on the phase-field method is described. In addition to long range order parameters used to describe the orientation difference of hydrides and the conserved parameter used to represent the hydrogen concentration, the plastic strains were adopted as new order parameters to describe the plastic deformation around the hydrides. The simulation results showed that the plastic deformation decreases the stress level around hydrides significantly. Moreover, the externally applied stress not only plays an important role in the morphological evolution of hydride precipitation, but also results in tensile stresses inside hydride particles, which may cause crack initiation at the hydrides.

1. Introduction

As primary structural materials in the nuclear power industry, zirconium and its alloys have excellent characteristics, such as good mechanical properties, corrosion resistance and low neutron absorption cross-section. However, zirconium has a strong affinity for hydrogen, and it will gradually pick up hydrogen from the service environment. As a result, the brittle zirconium hydride particles will form in zirconium and its alloys when the hydrogen concentration reaches a certain level. With the growth of hydride particles, a non-uniform internal stress field will be produced, and micro cracks may nucleate and propagate in the structure, resulting in the degradation of mechanical properties of the materials. For example, the fracture strength of the alloys can be reduced by orders of magnitude. It is a general consensus that critical conditions for the fracture initiation at hydrides are controlled by the morphology and microstructure of hydride precipitates. Therefore, the ability of predicting the morphology and microstructure evolution of hydride precipitation may play an important role in the reliability and safety assessment of zirconium structures.

In situ experimental study of the morphological evolution of hydride precipitates is an important way to investigate the failure mechanism of hydride-induced fracture in irradiated materials. Early experimental investigations [1–4] on hydride morphologies in zirconium and zirconium alloys showed a habit plane of $\{10\bar{1}0\}$ type and needle-like γ-hydrides growing in $\langle 11\bar{2}0\rangle$ directions. Experiments also showed that applied stress plays an important role in the morphology of hydrides. The tensile stress tends to change the orientation of habit planes so that the needle-like hydrides orient perpendicularly to the tensile direction. A threshold stress might be necessary in order for the hydrides to reorient themselves. In general, experimental study of hydride morphology and microstructure evolution in irradiated materials is rather expensive. Moreover, most observations were made on the surface of the specimen, and sectioning the specimen into bulk can only provide a 'snap shot' of the morphology at a given moment of the evolution.

On the other hand, due to the complexity of the problem, early theoretical studies had made simplified assumptions such as that the hydrides at a crack tip is a rectangular plate, see for examples, [5–9]. A theoretical model capable of predicting a multi-dimensional morphological evolution of hydrides had not been accomplished until 2000. Since 2000, we have been working on developing a theoretical framework for the realistic prediction of multi-dimensional hydride morphology evolution in zirconium using the phase-field method (PFM). The three key processes, namely, hydrogen diffusion, hydride phase transformation, and hydride fracture will be included in this framework.

PFM is a powerful computational approach to model and predict mesoscale morphological and microstructure evolution in materials [10]. In PFM, the compositions and phases (microstructures) in a system are described by a set of conserved and non-conserved field variables that are continuous across the interfacial regions. These field variables are assumed to follow the

* Corresponding author. Tel.: +852 2766 7821; fax: +852 2365 4703.
E-mail address: mmsqshi@polyu.edu.hk (S.Q. Shi).

0022-3115/$ - see front matter © 2008 Elsevier B.V. All rights reserved.
doi:10.1016/j.jnucmat.2008.05.008

time-dependent Ginzburg–Laudau dynamic equations (also called non-linear Langevin equations for non-conserved variables, and Fick's diffusion equations for conserved variables). For simplicity, our early work only considered linear elastic deformation in the hydrides and in zirconium matrix [11–14], and the simulation results on the hydrogen diffusion and hydride precipitation in zirconium under uniformly and non-uniformly applied stress were very encouraging. However, both experimental observations and numerical simulations showed that the maximum stress around hydrides in zirconium is greater than the yield stress of the matrix, i.e., plastic deformation in zirconium will take place during phase transformation. Furthermore, stresses at flaws such as at crack or notch tips may also exceed the yield stress. Therefore, it is necessary to appropriately account for the effect of plastic deformation in our theoretical framework. In this paper, an elastoplastic phase-field model is described and the predictions of the morphology evolution of hydride precipitation in zirconium using this new model will be compared with the ones obtained from the linear elastic method.

2. The elastoplastic phase-field model for specimens without flaws

We will take γ-hydrides as the example. Other types of hydrides (δ and ε) can be easily modeled using the same procedures. In fact, the simulations on polycrystalline zirconium described in the next section are also good for δ-hydrides as long as the simulation is in a two-dimensional space. The γ-hydrides are formed as a result of high cooling rates and have a face-centered tetragonal structure. If observed in (0001) plane of zirconium hexagonal matrix, they appear needle-like with axis along three $\langle 11\bar{2}0\rangle$ directions [1]. Within the face-centered tetragonal lattice, hydrogen atoms only occupy four tetrahedral interstitial positions, leaving the other four tetrahedral positions empty. As in the elastic phase-field model [11,12], we use the non-conservative structural field variables $\eta_p(\mathbf{r},t)$ ($p = 1, 2, 3$) to characterize the three orientation variants of γ-hydrides along three $\langle 11\bar{2}0\rangle$ directions. For a given orientation of needle-like hydrides, $\eta_p(\mathbf{r},t) = 1$ or -1 represents the two types of γ-hydrides in which a different set of tetrahedral positions is occupied by hydrogen, respectively. $\eta_p(\mathbf{r},t) = 0$ corresponds to a state of no γ-hydrides formed. According to the phase-field methodology, $\eta_p(\mathbf{r},t)$ have been assumed to follow the Langevin dynamic equations; while the conserved field variable, hydrogen concentration in the matrix and in the hydrides $c(\mathbf{r},t)$, is assumed to obey the generalized Fick's diffusion equation

$$\frac{\partial \eta_p(\mathbf{r},t)}{\partial t} = -L_p \frac{\delta F}{\delta \eta_p(\mathbf{r},t)} + \zeta_p(\mathbf{r},t) \quad (p = 1,2,3), \tag{1}$$

$$\frac{\partial c(\mathbf{r},t)}{\partial t} = M\nabla^2 \frac{\delta F}{\delta c(\mathbf{r},t)} + \xi(\mathbf{r},t), \tag{2}$$

where L_p and M are kinetic coefficients characterizing structural relaxation and diffusion mobility, respectively. Note that M has been assumed to be a weak function of hydrogen concentration and location. The noise terms $\zeta_p(\mathbf{r},t)$ and $\xi(\mathbf{r},t)$ follow Gaussian distribution and satisfy the requirements of the fluctuation–dissipation theorem. F is the total free energy of the system that includes chemical free energy for phase transformation, interface energy between matrix and hydride particles, and strain energy

$$F = \int \left\{ f_0(c(r),\eta_p(r)) + \sum_{p=1}^{3} \frac{\kappa_p}{2}[\nabla \eta_p(r)]^2 + \frac{\kappa_c}{2}[\nabla c(r)]^2 \right\} \mathrm{d}^3 r + E, \tag{3}$$

where f_0 is the local specific chemical free energy, κ_p and κ_c are gradient energy coefficients for orientation fields and composition field, respectively. The cross gradient energy terms are neglected for simplicity, and the integration is performed over the entire system. The two gradient terms are used to represent the interfacial energy between hydrides and matrix. E is the strain energy of the whole system. Eq. (1) simply says that the formation of hydride phase is determined by the minimization of total system energy, with $\delta F/\delta \eta_p = 0$ representing the final equilibrium state.

First, the local specific chemical free energy may be approximated using a Landau-type of free energy polynomial

$$f_0(c,\eta_p) = \frac{A_1}{2}(c-c_1)^2 + \frac{A_2}{2}(c-c_2)\sum_{p=1}^{3}\eta_p^2 - \frac{A_3}{4}\sum_{p=1}^{3}\eta_p^4 + \frac{A_4}{6}\sum_{p=1}^{3}\eta_p^6 + A_5\sum_{p\neq q}^{3}\eta_p^2\eta_q^2 + A_6\sum_{p\neq q, p\neq r}^{3}\eta_p^4(\eta_q^2+\eta_r^2) + A_7\sum_{p\neq q\neq r}^{3}\eta_p^2\eta_q^2\eta_r^2, \tag{4}$$

where c_1 and c_2 are the equilibrium concentrations of hydrogen in matrix and in hydrides, respectively. A_i ($i = 1,\ldots,7$) are phenomenological constants which are selected to satisfy the degenerate minima with respect to the order field variables at hydrogen concentrations c_1 and c_2. The values of $A_1 \sim A_4$ mainly determine the two minima in the specific chemical free energy at c_1 ($\eta_p(\mathbf{r},t) = 0$) and c_2 ($\eta_p(\mathbf{r},t) = 1$ or -1); while a proper choice of $A_5 \sim A_7$ provides the insurance that two (or three) different hydride variants can not grow at the same location (otherwise the specific chemical free energy will increase significantly). The exact shape of the specific chemical free energy f_0 in (c, $\eta_p(\mathbf{r},t)$) space is not well known. However, the values of c_1 and c_2 for a given temperature in zirconium have been measured experimentally. Our main task in defining the values of $A_1 \sim A_7$ was to find the two minima accurately at c_1 ($\eta_p(\mathbf{r},t) = 0$) and c_2 ($\eta_p(\mathbf{r},t) = 1$ or -1).

The strain energy (E) should account for the volume expansions due to hydrogen interstitial atoms and hydride particles, the elastic interaction between hydrogen atoms and hydride particles, and the elastic interaction between these impurities and externally applied stresses. It is worthy to note that the strain energy should include not only elastic deformation, but also plastic deformation. According to the Khachaturyan–Shatalov (KS) theory [15,16], the strain energy of an anisotropic discontinuous body can be described equivalently by an anisotropic continuous body of the same macroscopic size and shape, but having heterogeneous misfit stress-free strains (some time also called eigen strains) at cracks, secondary phases and so on. The exact expression of strain energy under a stress-controlled boundary condition is given by a function of eigen strains ε_{ij}^0

$$E = \frac{1}{2}\int_V C_{ijkl}\varepsilon_{ij}^0(\mathbf{r})\varepsilon_{kl}^0(\mathbf{r})\mathrm{d}^3 r - \frac{1}{2V}C_{ijkl}\int_V \varepsilon_{kl}^0(\mathbf{r})\mathrm{d}^3 r \int_V \varepsilon_{kl}^0(r')\mathrm{d}^3 r' - \frac{1}{2}\fint_V \frac{\mathrm{d}^3 k}{(2\pi)^3} n_i \tilde{\sigma}_{ij}^0(k)\Omega_{jk}(n)\tilde{\sigma}_{kl}^0(k)^* n_l - \sigma_{ij}^{\mathrm{appl}}\int_V \varepsilon_{ij}^0(\mathbf{r})\mathrm{d}^3 r - \frac{V}{2}S_{ijkl}\sigma_{ij}^{\mathrm{appl}}\sigma_{kl}^{\mathrm{appl}}, \tag{5}$$

where V is the system volume; the integral $\fint$ in the infinite reciprocal space is evaluated as a principal value excluding the point $\mathbf{k} = 0$; $\Omega_{jk}(\mathbf{n})$ is the Green function tensor, which is the inverse of the tensor $\Omega_{jk}^{-1}(\mathbf{n}) = n_i C_{ijkl} n_l$; S_{ijkl} is the elastic compliance tensor inverse to the elastic modulus C_{ijkl}; $\mathbf{n} = \mathbf{k}/k$ is a unit directional vector in the reciprocal space; $\tilde{\sigma}_{ij}^0(\mathbf{k}) = C_{ijkl}\tilde{\varepsilon}_{kl}^0(\mathbf{k})$; $\tilde{\varepsilon}_{kl}^0(\mathbf{k})$ are the Fourier transforms of $\varepsilon_{kl}^0(\mathbf{r})$ (i.e., $\tilde{\varepsilon}_{kl}^0(\mathbf{k}) = \int \varepsilon_{kl}^0(\mathbf{r}) \cdot \exp(-i\mathbf{k}\cdot\mathbf{r})\mathbf{d}^3\mathbf{r}$); the superscript asterisk (*) indicates the complex conjugate; and $\sigma_{ij}^{\mathrm{appl}}$ is the applied external stress. According to KS theory, the first term in Eq. (5) denotes the energy required to squeeze the transformed phase particles, voids or cracks to provide an initial undistorted state (to restore their original shapes before the transformation). The second and third terms are the energy reductions due to the macroscopic

homogeneous relaxation and local heterogeneous strain relaxation of the squeezed state, respectively. The last two terms are the work done by the external load.

When a state of equilibrium is reached, the thermodynamic driving force becomes zero, and the total stress can be given by

$$\sigma_{ij}(r) = -\frac{\partial E}{\partial \varepsilon^0_{ij}(r)} = \int_V \frac{\mathrm{d}^3k}{(2\pi)^3}\left[\tilde{\sigma}^0_{ij}(\mathbf{k}) - C_{ijkl}n_k\Omega_{lm}(\mathbf{n})\tilde{\sigma}^0_{mn}(\mathbf{k})n_n\right]\exp(\mathrm{i}\mathbf{k}\cdot\mathbf{r}) + \sigma^{\mathrm{appl}}_{ij}. \tag{6}$$

In a system containing hydrides, hydrogen interstitial atoms in solid solution, and plastic deformation, the total eigen strains are given by

$$\varepsilon^0_{ij}(\mathbf{r}) = \sum_{p=1}^{3}\varepsilon^{\eta}_{ij}(p)\eta^2_p(\mathbf{r}) + \varepsilon^c_{ij}\delta c(\mathbf{r}) + \varepsilon^p_{ij}(\mathbf{r}), \tag{7}$$

where $\eta_p(\mathbf{r})$ is the normalized structural order parameter describing the pth variant and $\varepsilon^{\eta}_{ij}(p)$ is the corresponding stress-free strain of hydrides for the pth variant when $\eta_p(\mathbf{r}) = 1$; ε^c_{ij} is the stress-free strain caused by the lattice expansion due to hydrogen interstitials; $\delta c(\mathbf{r})$ is the hydrogen concentration difference related to average hydrogen concentration in zirconium matrix; and $\varepsilon^p_{ij}(\mathbf{r})$ is the plastic strain in matrix. Since there is little information about plastic deformation inside the hydrides in the literature, we assumed that hydrides can only deform elastically. As a result, $\varepsilon^p_{ij}(\mathbf{r})$ can be non-zero only outside the hydrides. In addition, experimental evidence showed that when hydride size is very small (in the order of nano-meters), it is not possible to generate plastic deformation around the hydrides because the necessary geometric condition for the formation of dislocations around hydrides is not met. Therefore, in the very early stage of our simulations (during the nucleation stage), $\varepsilon^p_{ij}(\mathbf{r})$ was treated as zero everywhere.

As one can see, the plastic strain has been treated as a 'new' secondary phase in the system. The stress-free strains $\varepsilon^{\eta}_{ij}(\mathbf{r})$ and $\varepsilon^c_{ij}(\mathbf{r})$ have been measured from experiments, while $\varepsilon^p_{ij}(\mathbf{r})$ has to be determined by mechanical deformation laws. The plastic deformation is driven by the reduction in distortion strain energy at the location of concern [17]. The distortion strain energy can be obtained by following a similar procedure for Eq. (5)

$$E^{\mathrm{dis}} = \frac{1}{2}\int_V C_{ijkl}e^0_{ij}(\mathbf{r})e^0_{kl}(\mathbf{r})\mathrm{d}^3r - \frac{1}{2}C_{ijkl}\int_V e^0_{kl}(\mathbf{r})\mathrm{d}^3r\int_V e^0_{kl}(\mathbf{r}')\mathrm{d}^3r' - \frac{1}{2}\int_V \frac{\mathrm{d}^3k}{(2\pi)^3}n_i\tilde{s}^0_{ij}(\mathbf{k})\Omega_{jk}(\mathbf{n})\tilde{s}^0_{kl}(\mathbf{k})^*n_l - s^{\mathrm{appl}}_{ij}\int_V e^0_{kl}(\mathbf{r})\mathrm{d}^3r - \frac{V}{2}S_{ijkl}s^{\mathrm{appl}}_{ij}s^{\mathrm{appl}}_{kl}, \tag{8}$$

where $e^0_{ij}(\mathbf{r}) = \varepsilon^0_{ij}(\mathbf{r}) - 1/3\varepsilon^0_{kk}(\mathbf{r})\delta_{ij}$ is the deviatoric strain, and the deviatoric stress in Fourier space is $\tilde{s}^0_{ij}(\mathbf{k}) = int_V C_{ijkl}\times e^0_{kl}(\mathbf{r})\exp(-\mathrm{i}\mathbf{k}\cdot\mathbf{r})\mathrm{d}^3r$. The evolution of the plastic zone can then be depicted by the solution of an additional Langiven equation [17]

$$\frac{\partial\varepsilon^p_{ij}(\mathbf{r}_p,t)}{\partial t} = -N_{ijkl}\frac{\delta E^{\mathrm{dis}}}{\delta\varepsilon^p_{kl}(\mathbf{r}_p,t)}, \tag{9}$$

where $\mathbf{r}_p$ denotes the domain of plastic deformation; in other words, the Eq. (9) is valid only for the points inside plastic zones; N_{ijkl} is a kinetic coefficient characterizing the structural evolution rate of plastic deformation. In fact, Eq. (9) can be regarded as another form of the classic Prandle–Reuss plasticity theory [18]. We have assumed an elastic–perfectly plastic stress–strain behavior for the zirconium matrix, which is a very good representation of the experimental observations. We also assumed that the absolute value of uniaxial yield stress of zirconium matrix is the same for tension or compression test. During our simulations, the von Mises yield criterion was applied at every location except inside the hydrides and at every time step after the nucleation stage. Once the von Mises criterion was exceeded, Eq. (9) was then used to determine the values of $\varepsilon^p_{ij}(\mathbf{r})$. This methodology was tested not only for uniaxial tension–compression simulations (which resulted in an expected plastic deformation loop in a stress–strain plot), but also for the plastic zone predictions around a crack or a hole [17].

The kinetic coefficients can change the evolution rate but can not change the final morphology of the system at equilibrium. There is little information on kinetic coefficients, L_p and N_{ijkl}, in the literature. Therefore, for simplicity, we assume that $N_{ijkl} = S_{ijkl}/t_0$, where $t_0 = L_p mk_{\mathrm{B}}T^{-1}$. The evolution of hydride precipitation in zirconium without the presence of voids or cracks can be described by the simultaneous solution of Eqs. (1), (2) and (9). Since the above equations are non-linear with respect to the field variables, more efficient and accurate semi-implicit Fourier-spectral algorithms have been implemented [19].

3. Simulation results and discussion

The simulations of hydride precipitation were conducted in a 2D representative volume element (RVE) with 256×256 uniform grids, although the formulations described in section 2 are also good for 3D simulations. The c-axis of the hexagonal Zr crystal is normal to the 2D plane. The parameters $A_1 \sim A_7$ in the free energy expression (4) were obtained by fitting to the phase diagram of the Zr–H system at about 250 °C. The parameters used in the phase-field simulation are given as follows: $A_1 = 18.5$, $A_2 = -8.5$, $A_3 = 11.5$, $A_4 = 4.5$, $A_5 = A_6 = A_7 = 1.0$, all in the unit of $10^7\ \mathrm{J\,m^{-3}}$, $\kappa_p = \kappa_c = 1.5\times10^7\ \mathrm{J\,m^{-3}}$, $L_p = 0.4\ \mathrm{J^{-1}\,s^{-1}\,m^2}$, $M = 0.4\ \mathrm{J^{-1}\,s^{-1}}$, $N_{ijkl} = 1.0\ \mathrm{N\,m^{-2}\,s^{-1}}$, $c_1 = 0.006$, $c_2 = 0.59$. The elastic constants of zirconium are $C_{11} = 155.40$, $C_{12} = 68.03$, $C_{13} = 64.60$, $C_{33} = 172.51$, $C_{44} = 36.31$, $C_{66} = 44.09$, all in the unit of GPa [20]. Normalized time $t^* = t/t_0$ was used when solving the dynamic Eqs. (1), (2) and (9), and the iteration time step was $\Delta t^* = 0.001$.

To investigate the effect of plastic deformation on the evolution of hydride precipitation, one circular hydride seed with a radius of three grids was introduced into elastic and elastoplastic zirconium matrix, respectively. (It should be noted that the real γ-hydride nuclei may not be in circular shape. In later simulations, we will not pre-assume the shape of hydride nuclei.) The yield stress of unirradiated zirconium was assumed 540 MPa [21]. We assume that the plastic deformation only takes place in zirconium, not in hydrides. The transformation of tetragonal γ-hydride precipitates from hexagonal zirconium generates three possible equivalent orientation variants. The stress-free transformation strains caused by the hydride formation for the first orientation variant are 0.00551, 0.0564 and 0.0570 in $[1\,1\,\bar{2}\,0]$, $[1\,\bar{1}\,0\,0]$ and $[0\,0\,0\,1]$ direction, respectively. The eigen strains for the other two orientations can be obtained by rotating the first one about the c-axis by $2\pi/3$ and $-2\pi/3$, respectively. The stress-free transformation strains caused by hydrogen interstitials in Zr are $\varepsilon_{11} = \varepsilon_{22} = 0.0329$, and $\varepsilon_{33} = 0.0542$. The initial hydrogen concentration in the matrix was assumed 0.1, and the field variables (η_1, η_2, η_3) for the hydride were set as (1, 0, 0). To simulate the hydrogen ingress from environment, one needs to add a source term on the right-hand side of Eq. (2).

For a period of 5000 time steps, the circular seed has evolved into needle-like hydride particles because of the crystallographic anisotropy of transformation strain, as shown in Fig. 1. The x-axis is along $[1\,1\,\bar{2}\,0]$ direction and the y-axis is along $[1\,\bar{1}\,0\,0]$ direction. The distribution of stress σ_{yy} and von Misses stress σ_{m} in elastic and elastoplastic matrix are shown in Figs. 2 and 3, respectively. One can see that the maximum values of stresses are decreased

significantly due to the plastic deformation in zirconium matrix. This results in the decrease of hydrogen concentration near the two ends of the hydride, which results in a reduction of the length of the hydride particle for the same period of time of growth, as shown in Fig. 4. The growth of the hydride particle causes large tensile stresses in the matrix around two ends of needle-like particle and compressive stresses on the two sides of the hydride as well as inside the hydride. In general, both strain energy and interfacial energy will contribute to the morphology of hydride precipitation. Since the interfacial energy was assumed to be isotropic, the morphology of the hydride particle is dominantly determined by the strain energy that is in turn determined by the anisotropic eigen strains.

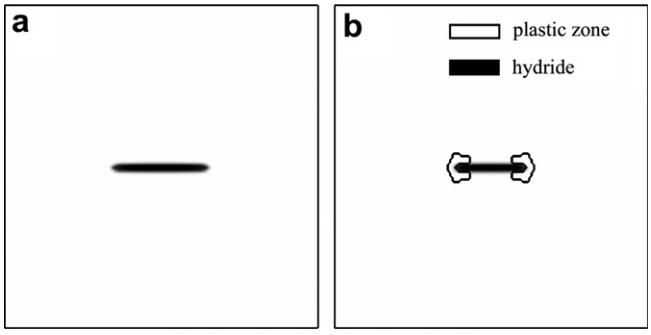

Fig. 1. The shape of a hydride particle simulated by PFM for 5000 time steps (a) in elastic matrix and (b) in elastoplastic matrix and corresponding plastic zone.

For the irradiated zirconium in nuclear power plants, the yield stress of the zirconium may increase to as much as 800 MPa [21]. As a result, the peak stress increases significantly, while the change in the distribution of hydrogen concentration is not evident, as shown in Fig. 5. This is due to the fact that the distribution of hydrogen concentration is determined by the distribution of the hydrostatic stress $\frac{1}{3}(\sigma_{xx}+\sigma_{xx}+\sigma_{yy})$, not by the stress distribution itself. In fact, the patterns of distributions of hydrogen concentration in Fig. 4 are very similar to that of distributions of hydrostatic stresses around the hydrides. In the following simulations, the yield stress of zirconium was assumed to be 540 MPa.

The evolution of three hydride particles after 5000 time steps is shown in Fig. 6. The particles become needle-like and grow along the three $\langle 1\,1\,\bar{2}\,0\rangle$ directions. The growth rate of hydride particles in the elastoplastic matrix is lower than that in the elastic matrix. Fig. 6(b) shows the plastic zone around the precipitation variants.

Since the hydrogen atoms in γ-hydride tetragonal lattice only occupy four tetrahedral sites and leave the other four tetrahedral sites empty [1], therefore, for the same orientation variant, there are two possible ways of arranging hydrogen atoms in γ-hydrides. We use $\eta_p = 1$ to represent one way and $\eta_p = -1$ to represent the other. When two hydrides with the same η_p meet each other (called in-phase), they coalesce to form a larger hydride, while when two hydrides with different η_p meet (called anti-phase), they will be separated by a grain boundary similar to stacking fault interface in crystals. In order to investigate the interaction among

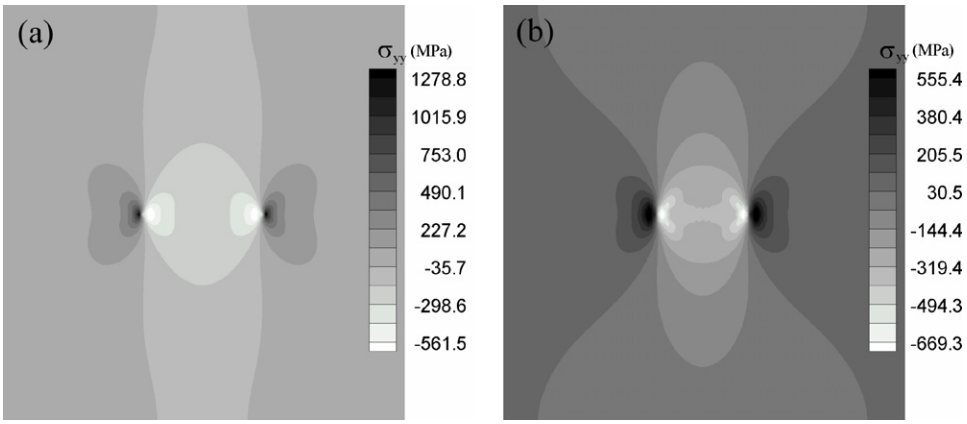

Fig. 2. The distribution of stress η_{yy} (a) in elastic matrix and (b) in elastoplastic matrix.

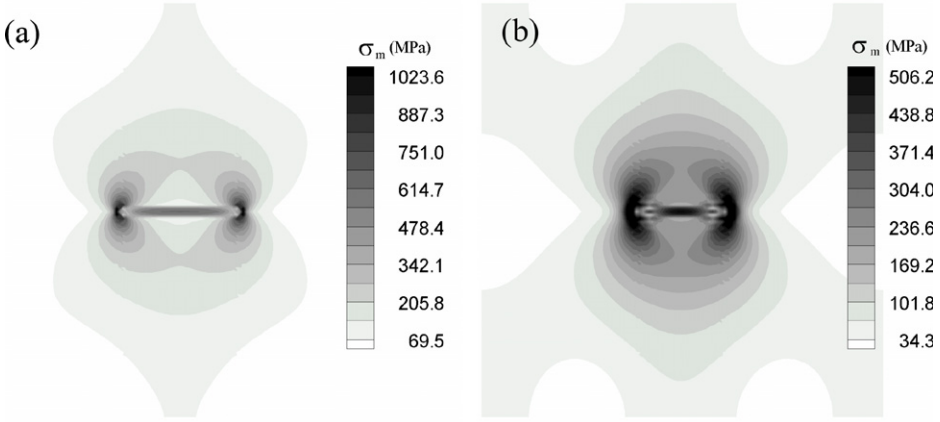

Fig. 3. The distribution of von Misses stress σ_m (a) in elastic matrix and (b) in elastoplastic matrix.

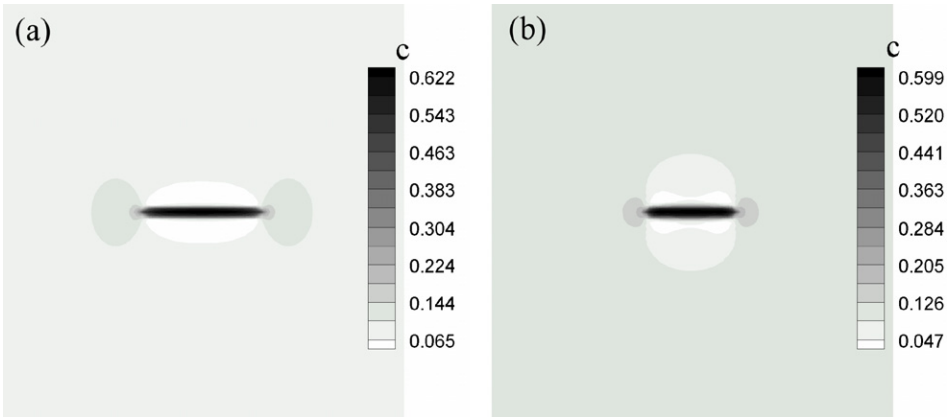

Fig. 4. The distribution of hydrogen concentration (a) in elastic matrix and (b) in elastoplastic matrix.

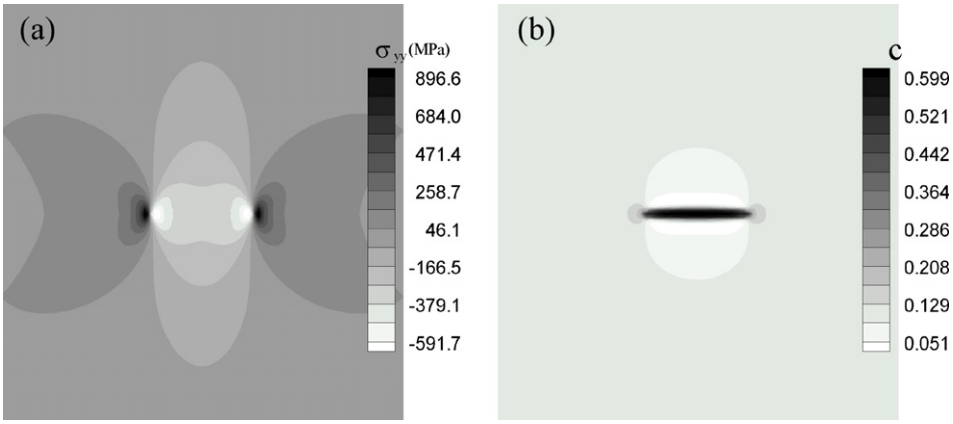

Fig. 5. (a) The distribution of stress σ_{yy} and (b) hydrogen concentration c when the yield stress of zirconium is increased to 800 MPa.

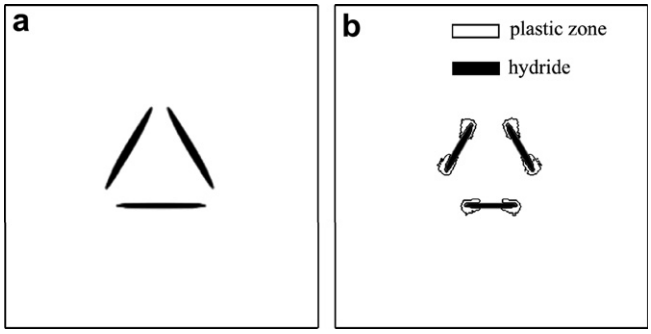

Fig. 6. (a) The shape of three hydride variants evolved in elastic matrix for 5000 time steps and (b) the shape of three hydride variants and plastic zone in elastoplastic matrix simulated by PFM for 5000 time steps.

the precipitation particles, two hydride seeds were placed in the RVE and separated by a distance of 30 grids in x-direction and three grids in y-direction between them. Depending on the initial values of η_p, the two hydrides will grow and meet each other either in-phase, or anti-phase, as shown in Figs. 7 and 8, respectively. In the in-phase situation, the two hydride particles merged into a larger one after 6000 time steps. By contrast, in the anti-phase situation, when the particles meet together they stop expanding at the contact end and leave an anti-phase grain boundary between them. This is more clearly seen in Figs. 9 and 10 for hydrostatic

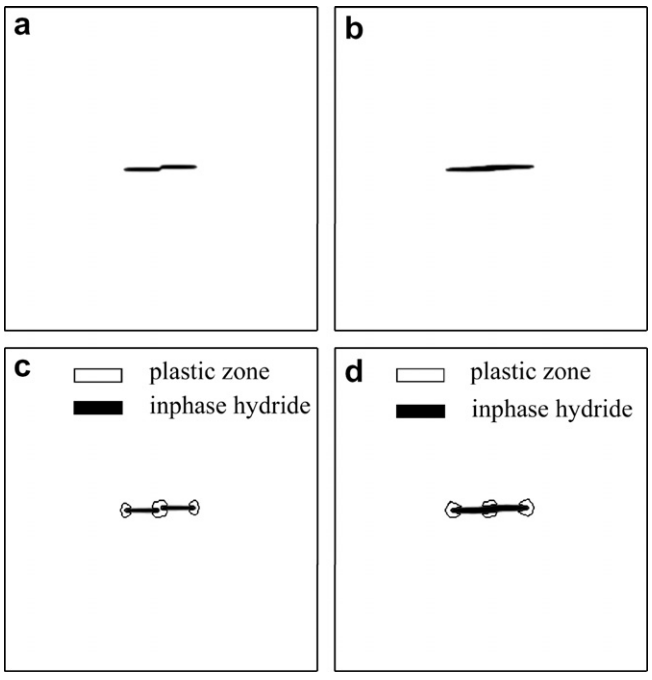

Fig. 7. The morphology evolution of two in-phase particles in elastic matrix (a) $t^* = 4000$ and (b) $t^* = 6000$; in elastoplastic matrix (c) $t^* = 4000$ and (d) $t^* = 6000$ and corresponding plastic zones.

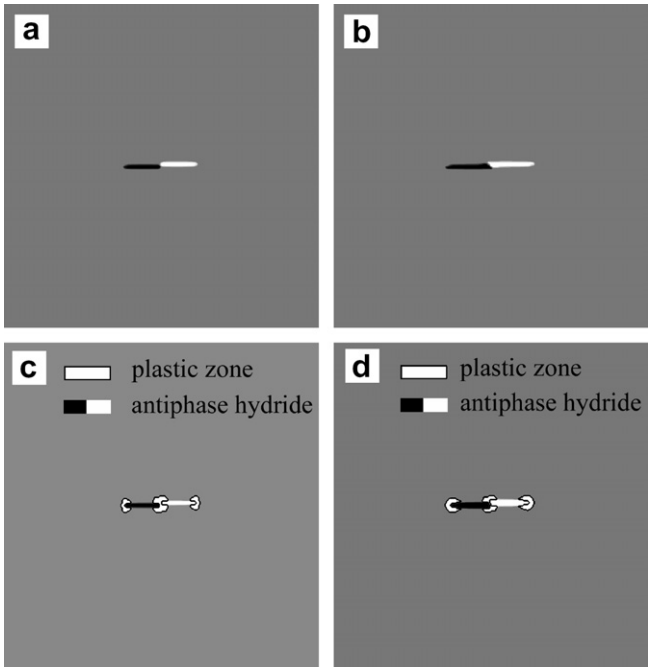

Fig. 8. The morphology evolution of two anti-phase particles in elastic matrix (a) $t^* = 4000$ and (b) $t^* = 6000$; in elastoplastic matrix (c) $t^* = 4000$ and (d) $t^* = 6000$ and corresponding plastic zones.

stress distribution around two hydrides. However, the magnitude of the stresses does not depend on whether it is in-phase or anti-phase. It is the yield stress of the matrix that controls the magnitude of the stresses around the hydrides.

In general, the stresses such as σ_{yy} inside horizontally aligned hydrides are normally negative (compressive) due to the volume expansion during hydride growth. However, if several hydride particles growing along different directions meet each other, the strain field interaction between them will affect the morphology of the hydrides and more importantly, the stress level inside the hydrides, as shown in Figs. 11 and 12. In some situations, a tensile stress may appear inside a hydride due to other neighbor hydrides. The maximum tensile stress in hydride particles observed in our simulation is about 870 MPa in the case of an elastic zirconium matrix, and about 500 MPa for an elastoplastic one. Such a tensile stress level inside a hydride may already be sufficient to cause fracture of the hydride, which will result in the initiation of microcracks in the structure.

The above simulations were done within a single crystalline zirconium, while real materials used in nuclear power plants are polycrystalline. We assume here that the average grain size of a polycrystalline zirconium is much smaller than the average size of the hydrides. This is a good approximation for the radial–circumferential plane in a pressure tube used in CANDU® nuclear power plants. We also assume that the material is isotropic (i.e., texture is ignored). (A true polycrystalline material with texture can be simulated using the same methodology with a much higher computational power.) To mimic this type of polycrystalline

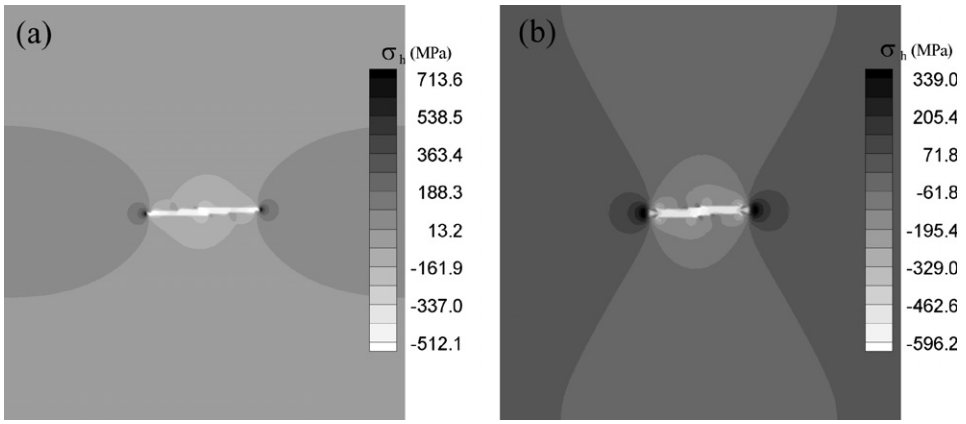

Fig. 9. Hydrostatic stress distribution around two in-phase hydrides (a) in elastic matrix and (b) in elastoplastic matrix.

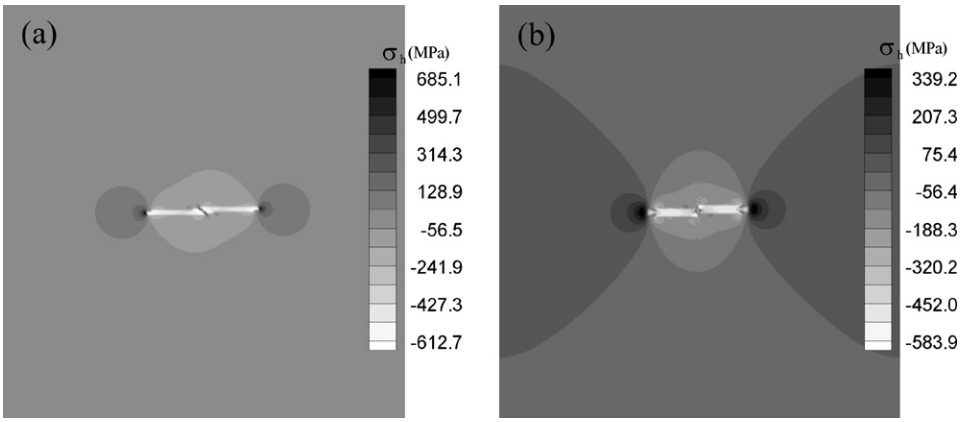

Fig. 10. Hydrostatic stress distribution around two anti-phase hydrides (a) in elastic matrix and (b) in elastoplastic matrix.

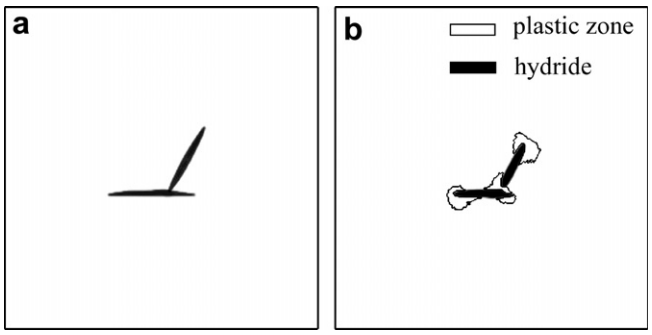

Fig. 11. The morphology shape of two hydride precipitation variants (a) in elastic matrix and (b) in elastoplastic matrix and corresponding plastic zone.

materials, the long range order parameters η_p should not be limited in three directions only. In other words, the orientation of the habit planes of γ-hydrides can be in any directions. The simulation results in the following are also good for δ-hydrides as long as the plate normal of δ-hydrides is within the 2D plane (i.e., the radial–circumferential plane of a pressure tube in CANDU® reactors).

In order to reduce the computing time, nine equally separated directions were selected in the 2D plane for η_p with $p = 1,2,3,\ldots,9$. As a result, one needs to solve six additional dynamic equations of the type Eq. (1). Instead of using C_{ijkl} to represent the modulus of a single crystal matrix, a Young's modulus of 81.5 GPa and Poisson's ratio of 0.33 were used for the isotropic matrix in following simulations. Fig. 13 shows nine hydrides growing in the nine directions in either elastic matrix or elastoplastic

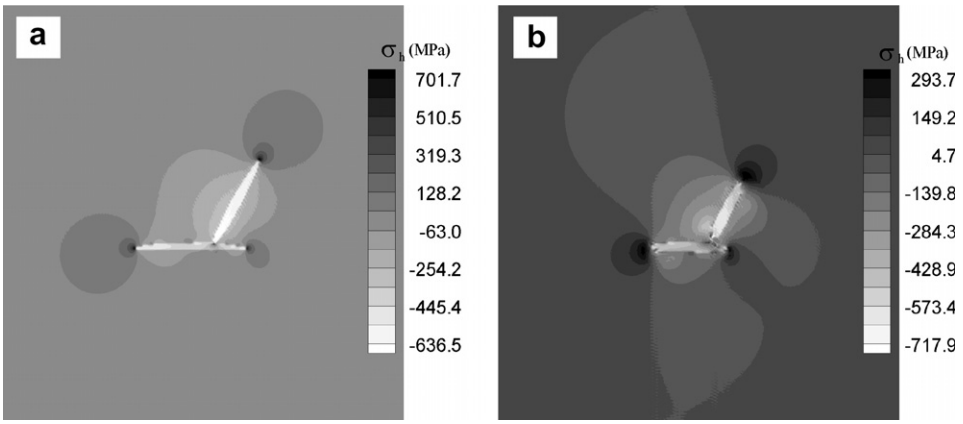

Fig. 12. The hydrostatic stress distribution around two hydride precipitation variants (a) in elastic matrix and (b) in elastoplastic matrix.

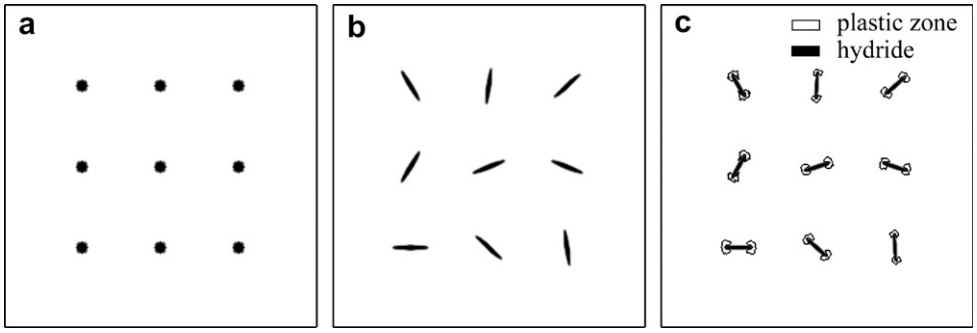

Fig. 13. The morphology evolution of hydrides simulated by PFM for 5000 time steps (a) the initial γ-hydride seeds, (b) shape change in elastic matrix and (c) shape change in elastoplastic matrix and corresponding plastic zones.

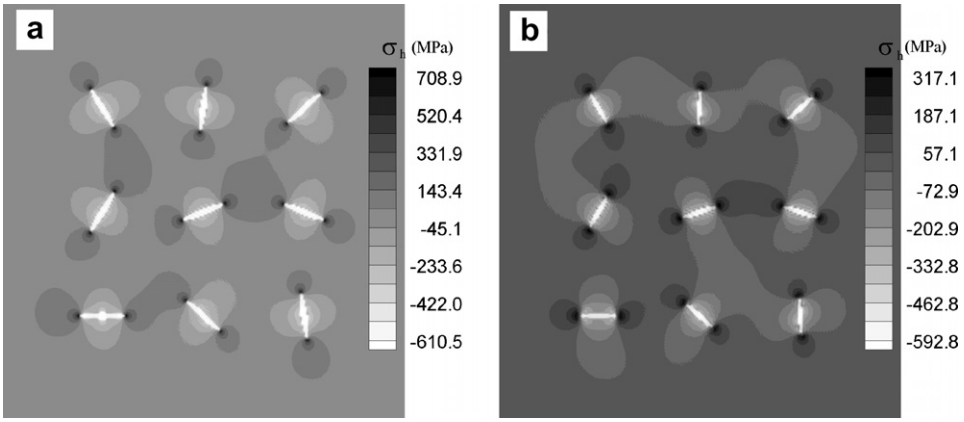

Fig. 14. Hydrostatic stress distribution (a) in elastic matrix and (b) in elastoplastic matrix.

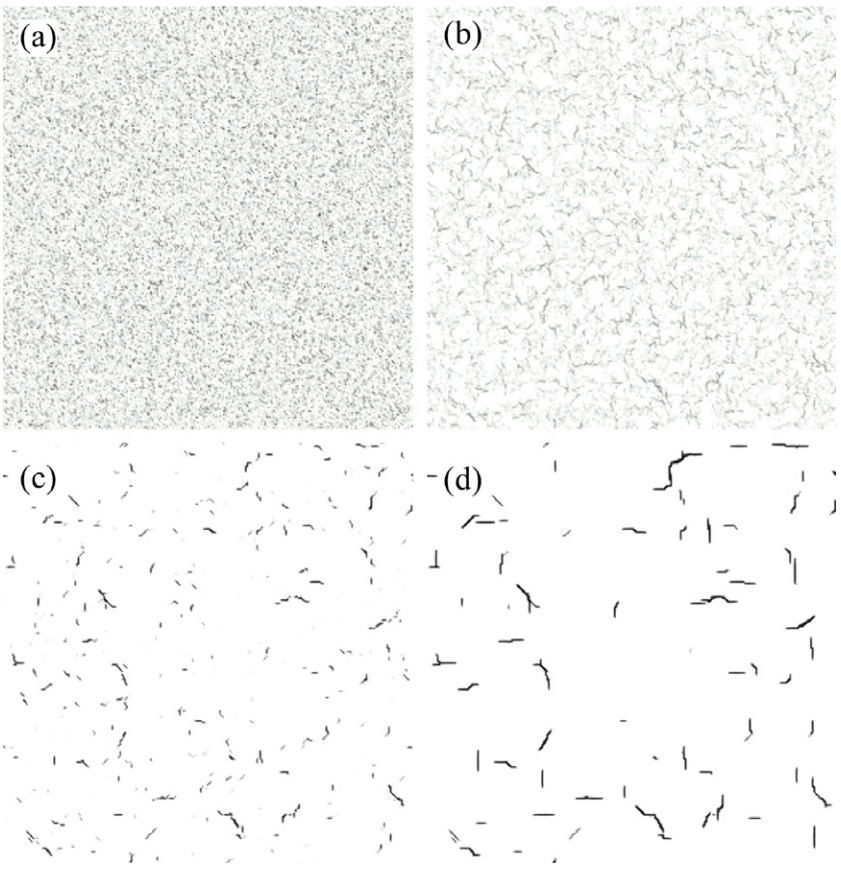

Fig. 15. The hydride precipitation process of γ -hydride in continuum matrix. (a) $t^* = 1000$, (b) $t^* = 2000$, (c) $t^* = 3000$ and (d) $t^* = 5000$.

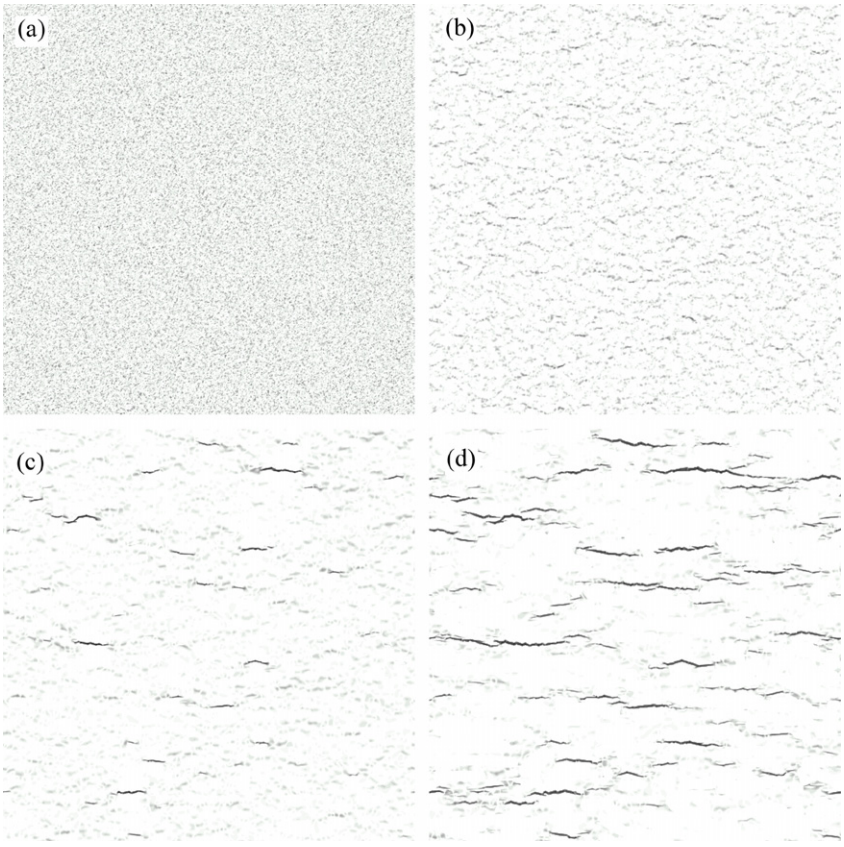

Fig. 16. γ-Hydride precipitation under external stress (200 MPa) applied vertically. (a) $t^* = 1000$; (b) $t^* = 2000$; (c) $t^* = 3000$; and (d) $t^* = 6000$.

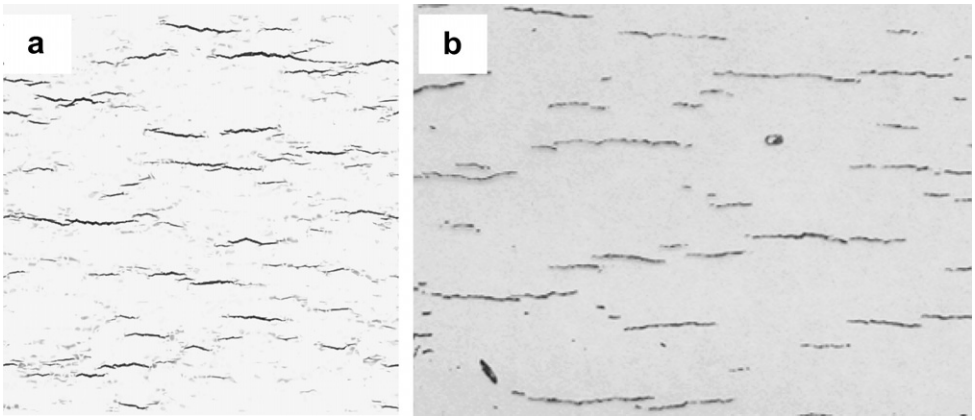

Fig. 17. Comparison of computer simulation (a) with experimental observation (b) (optical image) of hydride precipitation under uniformly applied tensile stress in vertical direction [22].

matrix. After 5000 time steps, the particles evolved into needle-like shape along different directions. Since the interfacial energy was assumed to be isotropic, the strain energy is dominant in hydride morphology. Similar to the single crystalline case, the evolution rate of hydride precipitation in elastoplastic matrix is slower than that in an elastic one. As a result, the length of needle-like hydride precipitates is shorter for the same evolution time. The plastic deformation takes place around the ends of needle-like hydride particles, as shown in Fig. 13(c). Fig. 14 shows the distribution of hydrostatic stresses in both cases. One can see that the magnitude of hydrostatic stress is decreased significantly due to the plastic deformation in matrix.

To simulate the complete process of hydride precipitation from nucleation, to growth and to coalescence, all the values of $\eta_p(\mathbf{r}, t)$ were initially set to be zero in the RVE with 512×512 uniform grids. The noise terms in dynamic Eqs. (1) and (2) were turned on during the first 1000 time steps to mimic the thermal fluctuation, then turned off afterwards. From Fig. 15, one can see that hydride nuclei larger than a critical size will grow along habit planes. Coalescence of hydride particles took place in later stage, while some smaller nuclei disappeared. The growth of different precipitation variants and their mutual positions are strongly dependent on the long range interaction of strain fields between them, as well as on the availability of hydrogen atoms in solid solution.

The effect of externally applied stress on the growth of hydride precipitation was also investigated by the phase-field model. Fig. 16 shows a case in which a vertical tensile stress of 200 MPa was applied to the RVE. One can see that the hydrides with the habit planes perpendicular to the tensile stress grow preferentially. Other orientation variants are not preferred due to higher strain energy, therefore almost disappeared. Under the externally applied tensile stress, the nucleation rate of hydride precipitates becomes higher. Large hydrides grow even larger at the expense of nearby smaller hydride particles. Therefore, the precipitation process proceeded in such a way that the total strain energy in the material is minimized. The simulated morphologies of the hydride precipitations agree well with that of experimental observations, as shown in Fig. 17 [22].

In the experiments conducted by Shi and Puls [22], the hydrides in smooth specimens without cracks were reoriented by a tensile stress during the cooling from high temperature at various cooling rates. The average hydride length was found to increase as a function of time spended during the cooling. Then the fracture strength of hydrides was measured by gradually increasing the tensile load and monitoring the acoustic emission at the same time. Their experimental results showed that, when the externally applied stress was up to about 640 MPa, the hydride cracking took place in the specimens where the average length of hydrides was between 25 and 90 μm (the maximum average length obtained by the experiments).

The phase-field simulation may help to identify the true fracture strength of these hydrides because the strain and stress at any location within a specimen are always calculated at any moment of the simulation (see for example, Eq.(6)). Using PFM, we first reorient the hydrides by applying a tensile stress of 200 MPa in a RVE without voids or cracks. After a long period of evolution time when the average length of hydrides does not change with time any more, the externally applied tensile stress (σ^{appl}) was increased to 640 MPa in the simulation and the average stress in all hydrides was calculated to be about 560 MPa. In fact, the differences between the average stresses in hydrides that were evolved for $t^* = 7000$, 8000, and 9000 are trivial.

A serious of simulations was performed to reorient hydrides for different evolution times under a tensile stress of 200 MPa, which results in different average lengths of hydrides. Then the growth of hydrides was stopped and the average stress in the hydrides was monitored when the applied tensile load was increased gradually. When the average stress in hydrides reached 560 MPa, the corre-

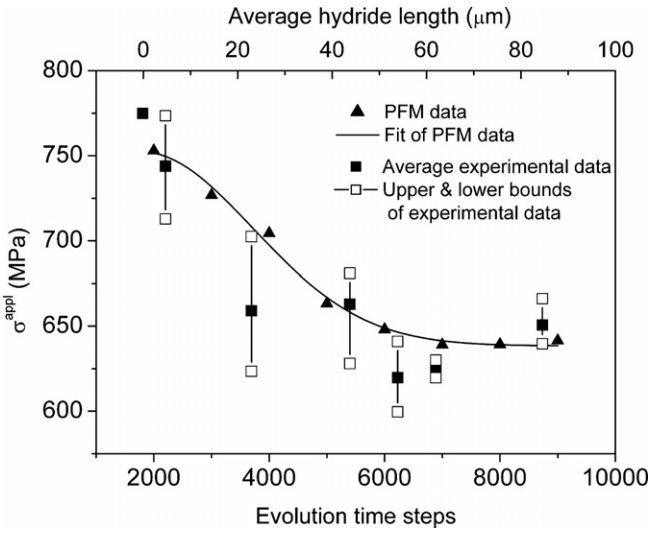

Fig. 18. The applied stress as a function of evolution time and average hydride length [22].

sponding applied tensile stress, σ^{appl}, was recorded and compared to the experimental data from Shi and Puls [22]. The comparison is given in Fig. 18. It can be seen that when the evolution time is short, the average hydride length is small, and a higher applied stress is needed to cause the hydride cracking. This example shows that a quantitative study can be conducted using PFM if suitable experimental data are available.

4. Conclusion

The morphological evolution of γ-hydride precipitation in zirconium matrix was simulated by a newly developed elastoplastic phase-field model. In addition to the conserved and non-conserved field variables that describe the hydrogen concentration and orientation of hydride precipitates respectively, the elastic and plastic strain were chosen as the field variables to describe the deformation of the matrix and the hydrides. The simulation results show that, due to the crystallographical anisotropy of transformation strain, the hydride particles evolve into needle-like in shape. As a result, compressive stresses will be produced inside the hydrides, while the zirconium matrix near the tips of hydride particles will be subjected to large tensile stresses, which leads to plastic deformations as well as attracts hydrogen atoms in solid solution. The plastic deformation significantly reduces the magnitude of stresses around the hydrides as compared to pure elastic deformation, which results in a reduced hydride growth. A tensile stress may appear inside a hydride if other nearby hydrides grow in different directions. The strain and stress at any location and at any moment in a specimen can be readily obtained by the PFM, which provides a convenient tool to study the fracture criteria of hydrides when compared to experimental results.

Acknowledgements

This work was supported by Grants from the Research Grants Council of Hong Kong (PolyU 5265/06E) for Shi, and from the National Natural Science Foundation of China (No. 10702007) for Guo.

References

[1] J.E. Bailey, Acta Metall. 11 (1963) 267.
[2] J.J. Kearns, C.R. Woods, J. Nucl. Mater. 20 (1966) 241.
[3] K.G. Barraclough, C.J. Beevers, J. Nucl. Mater. 34 (1970) 125.
[4] W.J. Babyak, Trans. AIME 239 (1967) 252.
[5] S.Q. Shi, M.P. Plus, J. Nucl. Mater. 208 (1994) 232.
[6] S.Q. Shi, M.P. Puls, S. Sagat, J. Nucl. Mater. 208 (1994) 243.
[7] S.Q. Shi, M. Liao, M.P. Puls, Model. Simul. Mater. Sci. Eng. 2 (1994) 1065.
[8] R. Dutton, M.P. Puls, in: A.W. Thompson, I.M. Bernstein (Eds.), Effect of Hydrogen in Behavior of Material, TMS AIME, New York, 1976, p. 516.
[9] W.J. Pardee, N.E. Paton, Metall. Trans. A. 11A (1980) 1931.
[10] L.Q. Chen, Annu. Rev. Mater. Res. 32 (2002) 113.
[11] X.Q. Ma, S.Q. Shi, L.Q. Chen, C.H. Woo, Comput. Mater. Sci. 23 (2002) 283.
[12] X.Q. Ma, S.Q. Shi, C.H. Woo, L.Q. Chen, Scripta Mater. 47 (2002) 237.
[13] X.Q. Ma, S.Q. Shi, S.Y. Hu, C.H. Woo, L.Q. Chen, J. University Sci. Technol. Beijing 12 (2005) 416.
[14] X.Q. Ma, S.Q. Shi, C.H. Woo, L.Q. Chen, Mech. Mater. 38 (2006) 3.
[15] A.G. Khachaturyan, Theory of Structural Transformations in Solids, Wiley, New York, 1983.
[16] Y.M. Jin, Y.U. Wang, A.G. Khachaturyan, Philos. Mag. 83 (2003) 1587.
[17] X.H. Guo, S.Q. Shi, X.Q. Ma, Appl. Phys. Lett. 87 (2005) 221910**.
[18] J. Chakrabarty, Theory of Plasticity, McGraw-Hill, New York, 1998.
[19] L.Q. Chen, J. Shen, J. Comput. Phys. Commun. 108 (1998) 147.
[20] M. Igarashi, M. Khantha, V. Vitek, N-Body interatomic potentials for hexagonal close-packed metals, Philos. Mag. B63 (1991) 603.
[21] M.P. Plus, J. Metall. Trans. A21 (1990) 2905.
[22] S.Q. Shi, M.P. Puls, J. Nucl. Mater. 275 (1999) 312.